Journal of Alloys and Compounds 521 (2012) 178–182

Contents lists available at SciVerse ScienceDirect

Journal of Alloys and Compounds

journal homepage: www.elsevier.com/locate/jallcom

Optical properties of iron oxide (α-Fe_2O_3) thin films deposited by the reactive evaporation of iron

M.F. Al-Kuhaili*, M. Saleem, S.M.A. Durrani

Physics Department, King Fahd University of Petroleum and Minerals, Dhahran 31261, Saudi Arabia

ARTICLE INFO

Article history:
Received 7 November 2011
Received in revised form 16 January 2012
Accepted 18 January 2012
Available online 27 January 2012

Keywords:
Iron oxide
Evaporation
Optical constants
Band gap

ABSTRACT

Thin films of hematite (α-Fe_2O_3) were deposited by the reactive evaporation of iron in an oxygen atmosphere. The films were deposited on unheated and heated substrates. Structural analysis, using X-ray diffraction, verified the phase of the films and revealed that the films had a polycrystalline structure composed of nano-crystallites. Atomic force microscopy indicated that the films had smooth surfaces, with a lateral grain size that increased substantially by substrate heating. The optical properties of the films, including the refractive index, extinction coefficient, absorption coefficient, and band gap were determined from spectrophotometric measurements. In the wavelength range 600–2000 nm, the refractive indices were 1.7–2.2 for the films deposited on unheated substrates, and 2.3–2.9 for the films deposited on heated substrates. The films had direct and indirect band gaps. The direct band gap was 2.18 eV, and the indirect band gap was 1.82–1.96 eV, depending on the substrate temperature.

1. Introduction

Iron can form several oxides of different stoichiometry and crystalline phases. These oxides are wustite (FeO), magnetite (Fe_3O_4), hematite (α-Fe_2O_3), and maghemite (γ-Fe_2O_3). Hematite is the thermodynamically stable phase of Fe_2O_3, and is the subject of this work. This material is a semiconductor that is characterized by good thermodynamic stability at high temperatures, non-toxicity, low cost and abundance [1]. From an optical point of view, α-Fe_2O_3 possesses a band gap (~2.2 eV) that lies in the visible range, and has a relatively high refractive index. Therefore, it has been investigated as a potential candidate for many optical applications, such as solar energy conversion, electrochromism, photocatalysis, interference filters, and photo-oxidation of water [1–4]. Hematite thin films have been prepared by a variety of techniques, including sputtering [2,5], sol–gel-deposition [6,7], spray pyrolysis [3,8,9], metalorganic deposition [10], electrodeposition [11], and pulsed laser deposition [12]. One of the simplest techniques for the preparation of α-Fe_2O_3 thin films is reactive evaporation, which requires no more than evaporation of pure iron in an oxygen atmosphere [4]. A similar technique is the oxidation of bulk iron substrates [13]. The drawback of this technique is that it is not useful for applications that require a transparent substrate.

Optical applications necessitate knowledge about the optical properties of the material. These include the refractive index (n), extinction coefficient (k), absorption coefficient (α), and the band gap (E_g). The optical properties of thin films are sensitively dependent on the preparation conditions and the models used to extract the optical constants from measured quantities. It is desirable to determine these properties as functions of the wavelength of light (or photon energy). In the case of the refractive index, such a relation constitutes the dispersion properties of the material. The dispersion relations were determined for α-Fe_2O_3 thin films deposited by sputtering [5], sol–gel [6,7], and spray pyrolysis [9]. The optical properties of titanium-doped α-Fe_2O_3, deposited by pulsed laser deposition, were reported [12]. Moreover, the optical constants of ultrathin α-Fe_2O_3 films were reported for films prepared by the oxidation of bulk iron [13]. Despite their potential optical applications and the large number of reports on the preparation of α-Fe_2O_3 thin films by reactive evaporation, the optical properties of these films have not been thoroughly investigated. In an earlier study, the refractive index was reported at a single spectral position [4]. It is worth mentioning that only in a few studies the obtained films were transparent, with transmittance exceeding 80% in the visible and near infrared ranges [3,4,10,12].

In this work, α-Fe_2O_3 thin films were prepared by the reactive evaporation of iron, both on heated and unheated substrates. First, the structural properties were investigated to verify the phase of the material and measure factors that affect the optical properties such as grain size and roughness. Then, the optical properties (n, k, α, E_g) were determined using the spectrophotometric method.

* Corresponding author. Tel.: +966 3 860 3747; fax: +966 3 860 2293.
E-mail address: kuhaili@kfupm.edu.sa (M.F. Al-Kuhaili).

0925-8388/$ – see front matter © 2012 Elsevier B.V. All rights reserved.
doi:10.1016/j.jallcom.2012.01.115

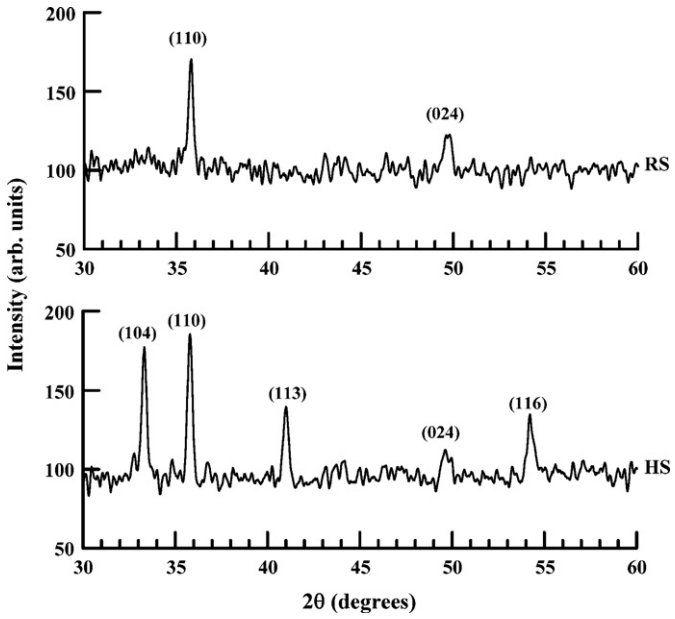

Fig. 1. XRD patterns of films deposited on unheated substrates (RS) and films deposited on substrates heated to 300 °C (HS).

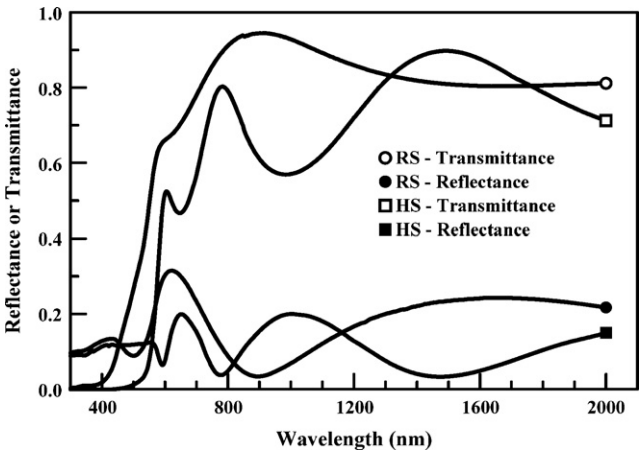

Fig. 3. Measured normal-incidence reflectance and transmittance spectra of the films. RS stands for films deposited on unheated substrates, and HS stands for films deposited on substrates heated to 300 °C.

2. Experimental

The starting material was solid iron granules (Alfa Aesar, purity 99.999%). Evaporation was done using electron-beam evaporation in a Leybold L560 box coater. The material was slowly out-gassed before evaporation. The system was pumped to a base pressure of 4×10^{-4} Pa. Then, oxygen was re-admitted into the deposition chamber. Deposition was carried out at an oxygen partial pressure of 0.1 Pa. The films were deposited on fused silica. The substrates were rotating during deposition, and the source-to-substrate distance was 40 cm. Two sets of films were deposited. The first set (RS films) was deposited on unheated substrates. The second set (HS films) was deposited on substrates that were heated to 300 °C. The evaporation rate (0.2 nm/s) and thickness of the films were controlled by a quartz crystal thickness monitor. The thickness of the films was measured using a surface profilometer (Ambios XP-2), and was also verified optically. The thickness of RS films was 241 nm, whereas the thickness of the HS films was 146 nm. The structure of the films was investigated by X-ray diffraction (XRD) using a Shimadzu XRD-6000 diffractometer, employing Cu Kα (1.54 Å) radiation. The surface morphology of the films was examined by tapping mode atomic force microscopy (AFM) (Veeco Innova diSPM). The sample surface was probed with a silicon tip of 10 nm radius oscillating at its resonant frequency of 300 kHz. The scan area was $2 \times 2\ \mu m^2$, and the scan rate was 1 Hz. Normal-incidence reflectance and transmittance were measured over the wavelength range 300–2000 nm using a Jasco V-570 double beam spectrophotometer.

3. Results

3.1. Structural properties

The XRD patterns of the films are shown in Fig. 1. The films had a polycrystalline structure. All of the observed peaks can be assigned to the α-Fe_2O_3 phase, in accordance with data from the International Center for Diffraction Data (ICDD file no. 01-071-5088). The films deposited on unheated substrates exhibited oriented growth along the (1 1 0) direction. On the other hand, the films deposited on heated substrates exhibited two preferred orientations, namely (1 0 4) and (1 1 0). The multiple growth directions for films deposited on heated substrates is due to the increased mobility of the atoms on the substrate's surface. The crystallite size was calculated using the Scherrerr equation, and was found to be 14 nm for RS films, and 15 nm for the HS films. Thus, the films had a nano-crystalline structure.

Atomic force microscopy images of the films are shown in Fig. 2. The surface morphology of the films showed columnar microstructure. Statistical analysis of the images was performed to obtain the root-mean-square surface roughness (R_{rms}) and lateral grain size of the films. The surface roughness was not affected by the substrate temperature (2.5 nm for the RS films, and 2.3 nm for the HS films). However, the lateral grain size showed significant dependence on substrate temperature (19.4 nm for the RS films, and 27.1 nm for the HS films). Heating the substrate increases the surface diffusion of the deposited species, and leads to coalescence of adjacent grains to form larger grains.

3.2. Optical constants

The measured reflectance and transmittance spectra of the films are shown in Fig. 3. The films deposited on unheated substrates had higher transmittance with shorter-wavelength absorption edges. The films deposited on heated substrates had larger grain sizes, and exhibited stronger polycrystalline growth. These factors enhance the scattering of light and reduce transmittance. The reflectance

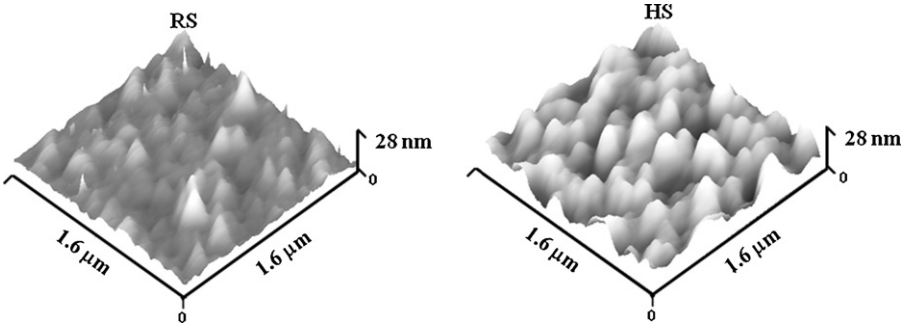

Fig. 2. Three dimensional atomic force images of films deposited on unheated substrates (RS) and films deposited on substrates heated to 300 °C (HS).

and transmittance spectra were characteristic of dielectric films, i.e. they had maxima and minima due to multiple-beam interference in the transparency region of the films.

In the transparency region of the films ($\lambda \geq 600$ nm), the transmittance spectra could be used to determine the optical constants of the films. The transmittance of a thin film on a transparent substrate is given by [14,15]:

$$T = \frac{16n_s(n^2+k^2)\beta}{A + B\beta^2 + 2\beta[C\ \cos(4\pi nd/\lambda) + D\ \sin(4\pi nd/\lambda)]} \quad (1)$$

with

$$A = [(n+1)^2 + k^2][(n+n_s) + k^2]$$
$$B = [(n-1)^2 + k^2][(n-n_s) + k^2]$$
$$C = -(n^2 - 1 + k^2)(n^2 - n_s^2 + k^2) + 4k^2 n_s$$
$$D = 2kn_s(n^2 - 1 + k^2) + 2k(n^2 - n_s^2 + k^2)$$

where n is the refractive index of the film, k is the extinction coefficient of the film, n_s is the refractive index of the substrate, d is the thickness of the film, λ is the wavelength of light, and $\beta = \exp(-4\pi kd/\lambda)$. The above equation refers to the transmittance of the film, which is obtained by dividing the measured transmittance by that of the substrate. In order to fit the experimental transmittance spectra using Eq. (1), models for the dispersion of n and k must be implemented. The refractive index of the films was modeled by a single oscillator model [16]:

$$n = \left(1 + \frac{E_o E_d}{E_o^2 - E^2}\right)^{1/2} \quad (2)$$

where E_o is the effective oscillator energy, E_d is the dispersion energy related to the interband transition strength, and E is the incident photon energy ($E = hc/\lambda$, where h is Planck's constant, and c is the speed of light in vacuum). The oscillator energy (E_o) is typically near the main peak of the imaginary part of the dielectric function [17]. The dispersion energy (E_d) is directly related to the structural order of the films, where it increases with enhanced crystallinity [17]. The extinction coefficient of the films was modeled by Urbach law of exponential absorption below the band gap [18]:

$$k = k_o\ \exp\left[\frac{E - E_1}{\delta}\right] \quad (3)$$

where k_o is a constant, E_1 is an energy representing the onset of absorption, and δ is the Urbach band energy width. The experimental transmittance spectra were fitted using Eq. (1), with Eqs. (2) and (3) as models for the optical constants. The fitting parameters were E_o, E_d, E_1, k_o, and δ. The substrate refractive index was taken from Ref. [19]. The calculated transmittance spectra, employing the above models for n and k successfully fitted the experimental spectra throughout the transparency range with a correlation that was better than 99%. The best-fit parameters are shown in Table 1, and they were used to calculate the optical constants of the films, which are shown by the dispersion curves of Fig. 4 (for n) and Fig. 5 (for k). Our results for the refractive index are compared with some of the reported values in Fig. 4. The values of the refractive index reported in the literature showed great variation based on the experimental technique and conditions, post-deposition treatment, and analytical techniques used to derive the refractive index.

Table 1
Summary of the best-fit parameters used in fitting the experimental transmittance spectra of the films.

Type	E_o (eV)	E_d (eV)	E_1 (eV)	δ (eV)	E_{gi} (eV)	E_{gd} (eV)	k_o
Unheated	2.94	5.42	2.23	0.12	1.82	2.18	0.17
Heated	3.16	13.04	2.21	0.75	1.96	2.18	0.02

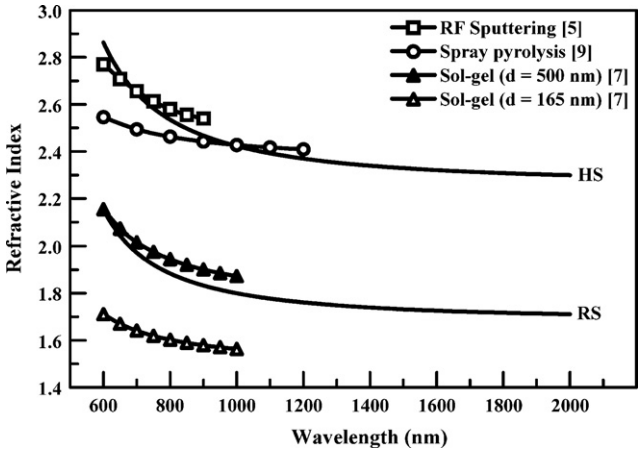

Fig. 4. Dispersion curves in the transparency region of the films. RS stands for films deposited on unheated substrates, and HS stands for films deposited on substrates heated to 300 °C. Values from the literature are included for comparison.

3.3. Band gap

The transmittance of a film can also be written as [20]:

$$T = \frac{(1-R)^2\ \exp(-\alpha d)}{1 - [R^2\ \exp(-2\alpha d)]} \quad (4)$$

where R is the reflectance of the film, and α is the absorption coefficient. In the fundamental absorption region ($\alpha > 10^4$ cm^{-1}), the second term in the denominator of Eq. (4) is negligible. Therefore, Eq. (4) can be rewritten as $T \approx (1-R)^2 e^{-\alpha d}$. From which,

$$\alpha = \frac{1}{d}\ \ln\left(\frac{(1-R)^2}{T}\right) \quad (5)$$

The absorption coefficient was calculated using Eq. (5), and the results are shown in Fig. 6. In the fundamental absorption region, the absorption coefficient is related to the band gap (E_g) by the relation [21]:

$$\alpha = \frac{\alpha_o}{E}(E - E_g)^\eta \quad (6)$$

where α_o is a constant with values between 10^5 and 10^6 cm^{-1} [21]. The constant η depends on the type of transitions involved: $\eta = 0.5$ corresponds to a direct allowed transition, and $\eta = 2$ corresponds to an indirect allowed transition. In order to obtain the band gap,

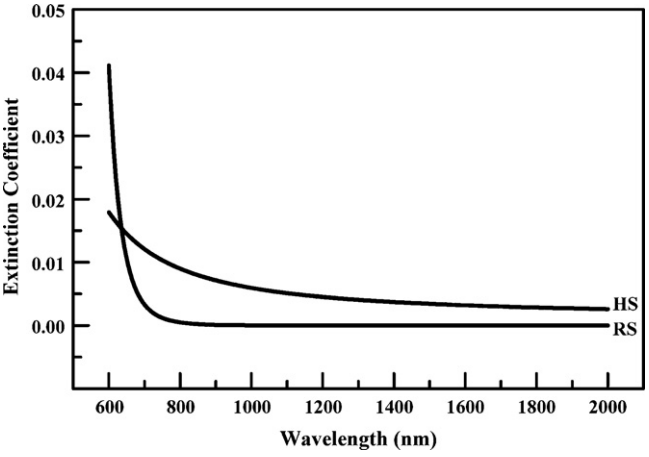

Fig. 5. Variation of the extinction coefficient with the wavelength of light. RS stands for films deposited on unheated substrates, and HS stands for films deposited on substrates heated to 300 °C.

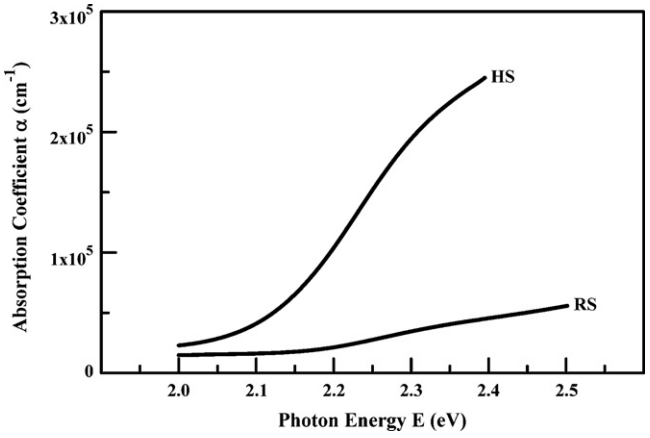

Fig. 6. Dependence of the absorption coefficients of the films on photon energy. RS stands for films deposited on unheated substrates, and HS stands for films deposited on substrates heated to 300 °C.

$(\alpha E)^{1/\eta}$ is plotted as a function of photon energy. The linear portions of the curves are fitted using linear regression analysis. An extrapolation of the linear regions of the plots gives the value of the band gap as the intercept to the horizontal axis (where $\alpha E = 0$). Such plots (called Tauc plots) are shown in Fig. 7. Both direct and indirect transitions were investigated. The resulting band gap values are given in Table 1, where E_{gi} denotes the indirect band gap and E_{gd} denotes the direct band gap. The indirect band gaps varied with the substrate temperature, whereas the direct band gaps did not show any variation.

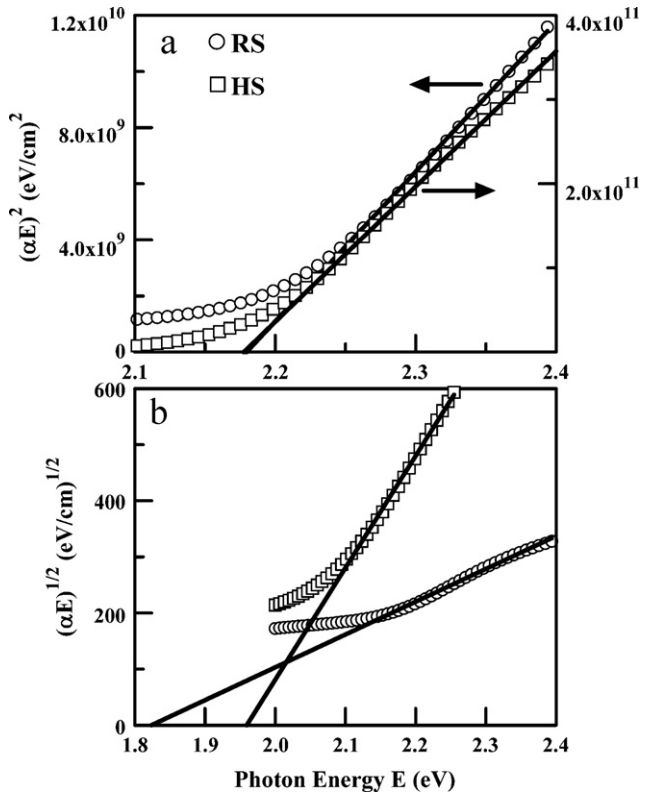

Fig. 7. Tauc plots of the films deposited on unheated substrates (RS) and films deposited on heated substrates (HS): (a) direct band gaps, and (b) indirect band gaps.

4. Discussion

The refractive index of the films deposited on heated substrates was much higher than those of films deposited on unheated substrates. A similar trend was shown for sputtered [5] and sprayed [9] films. The variation of the refractive index with substrate temperature may be correlated with the density of the films. The low value of the refractive index for the RS films indicates that these films had relatively low packing density. Lowering of the packing density is caused by the incorporation of oxygen during film growth [22], which may create voids that absorb moisture [23]. Moreover, collisions of the evaporated species with O_2 molecules reduce their kinetic energy before reaching the substrate, and this will result in lower packing density [23]. The increase of refractive index with substrate temperature may be attributed to an increase in the density of films deposited on heated substrates. Substrate heating provides thermal energy that increases the mobility of the atoms of the films, thereby increasing the packing density of the films [24]. This is supported by three observations. First, the thickness of the HS films was less than that of RS films. Second, the HS films had larger lateral grain size, indicating that there were less voids in these films due to the coalescence of the grains. Third, the dispersion energy (E_d) was larger for the HS films, which is also correlated with densification of the films [7]. An estimate of film density may be obtained from the Lorentz–Lorenz relation [25]:

$$\frac{\rho_f}{\rho_b} = \frac{(n_f^2 - 1)(n_b^2 + 2)}{(n_f^2 + 2)(n_b^2 - 1)} \tag{7}$$

where ρ_f is the density of the film, ρ_b is the density of the bulk material, n_f is the film's refractive index (Fig. 4), and n_b is the bulk refractive index whose value is 3.003 at $\lambda = 633$ nm [26]. Using n_f values of 2.075 (RS films) and 2.773 (HS films) at $\lambda = 633$ nm, the relative density (ρ_f/ρ_b) was 0.72 for the RS films, and 0.95 for the HS films; indicating the compact and dense nature of the HS films. The extinction coefficient was higher for the films deposited on heated substrates. Similar to the refractive index, the extinction coefficient increases for the higher-density films [27]. Dense packing will reduce the voids within the film and increase absorption. Moreover, the extinction coefficient of the HS films had non-zero values up to $\lambda = 2000$ nm, i.e. throughout the near-infrared range. This is also supported by the larger Urbach band energy width (δ) of these films, which indicates that absorption in these films extends well beyond the fundamental band gap. The major source of absorption in this spectral region is scattering, which may be substantial due to the larger grain size of these films.

Several studies reported that α-Fe_2O_3 has an indirect band gap [6,11]. Other studies reported a direct band gap of the material [7]. Some groups have also reported direct band gaps occurring in conjunction with indirect band gaps [1,3,8]. In this case, the direct band gap was attributed to quantum size effects associated with nanoparticles or naocrystallites. The reported values of the indirect band gap were in the range 1.38–2.09 eV [1–3,6,8,11]. The reported values of the direct band gap were in the range 1.95–2.35 eV [1,2,7,8]. Our values of the band gaps were in close agreement with the reported values. The increase of the indirect band gap with substrate temperature was also reported for sprayed α-Fe_2O_3 thin films [8], although the opposite trend was reported for sputtered films [2]. This is mainly attributed to changes in the crystalline structure as a result of substrate heating, which in turn depends on the crystalline structure of the as-deposited films on

unheated substrates, which is critically dependent on the deposition technique.

5. Conclusions

Hematite thin films (α-Fe_2O_3) were deposited by the reactive evaporation of iron under a partial pressure of 0.1 Pa of oxygen. Both unheated and heated (300 °C) substrates were used. Structural analysis of the films showed the following: (i) the films were polycrystalline, (ii) the films had nano-crystallite size of about 15 nm, (iii) the surface roughness was around 2.5 nm, and (iv) the lateral grain size was 19.4 nm for the films deposited on unheated substrates and 27.1 nm for the films deposited on heated substrates. The films deposited on heated substrates were compact with lower thickness. The optical constants were determined using the spectrophotometric method. Films deposited on unheated substrates had a refractive index ranging from 1.7 to 2.2 in the visible and near infrared wavelength range from 600 to 2000 nm. Over the same wavelength range, the films deposited on heated substrates had much higher values of the refractive index ranging from 2.3 to 2.9. This increase was correlated with the density of the films. Likewise, the extinction coefficient of the films deposited on heated substrates had higher values than that of films deposited on unheated substrates. In addition to density, this variation was attributed to increased absorption related to scattering. The films exhibited the presence of both direct and indirect band gaps. The direct band gap had a value of 2.18 eV for both types of films. The indirect band gap had a value of 1.82 eV for the films deposited on unheated substrates and a value of 1.96 eV for the films deposited on heated substrates. In conclusion, both types of films had a direct band gap value that renders them useful for solar energy conversion. However, the films deposited on heated substrates were more compact, which makes them less prone to environmental effects. Moreover, their much higher refractive index presents them as suitable candidates for high-index applications, such as interference filters and architectural glazing coatings.

Acknowledgment

Support for this work by the Physics Department of King Fahd University of Petroleum and Minerals is greatly acknowledged.

References

[1] N. Beermann, L. Vayssieres, S-E. Lindquist, A. Hagfeldt, J. Electrochem. Soc. 147 (2000) 2456.
[2] E.L. Miller, D. Paluselli, B. Marsen, R.E. Rocheleau, Thin Solid Films 466 (2004) 307.
[3] L. Dghoughi, B. Elidrissi, C. Bernede, M. Addou, M. Alaoui Lamrani, M. Regragui, H. Erguig, Appl. Surf. Sci. 253 (2006) 1823.
[4] Y.J. Park, K.M.A. Sobahan, C.K. Hwangbo, Surf. Coat. Technol. 203 (2009) 2646.
[5] K. Morl, U. Ropke, B. Knappe, J. Lehmann, R. Perthel, H. Schroder, Thin Solid Films 60 (1979) 49.
[6] N. Ozer, F. Tepehan, Sol. Energy Mater. Sol. Cells 56 (1999) 141.
[7] M. Gartner, M. Crisan, A. Jitianu, R. Scurtu, R. Gavrila, I. Oprea, M. Zaharescu, J. Sol–Gel Sci. Technol. 26 (2003) 745.
[8] A. Akl, Appl. Surf. Sci. 233 (2004) 307.
[9] A. Akl, Appl. Surf. Sci. 256 (2010) 7496.
[10] S. Xue, W. Ousi-Benomar, R.A. Lessard, Thin Solid Films 250 (1994) 194.
[11] G. Zotti, G. Schiavon, U. Casellato, J. Electrochem. Soc. 145 (1998) 385.
[12] C.X. Kronawitter, S.S. Mao, B.R. Antoun, Appl. Phys. Lett. 98 (2011) 092108.
[13] V. Goossens, J. Wielant, S. Van Gils, R. Finsy, H. Terryn, Surf. Interface Anal. 38 (2006) 489.
[14] O.S. Heavens, Optical Properties of Thin Solid Films, Dover, New York, 1991, p. 78.
[15] J.C. Manifacier, J. Gasiot, J.P. Fillard, J. Phys. E 9 (1976) 1002.
[16] S.H. Wemple, M. Didomenico, Phys. Rev. B 3 (1971) 1338.
[17] S. Zhao, F. Ma, K.W. Xu, H.F. Liang, J. Alloys Compd. 453 (2008) 453.
[18] M. Girtan, G. Folcher, Surf. Coat. Technol. 172 (2003) 242.
[19] I.H. Malitson, J. Opt. Soc. Am. 55 (1965) 1205.
[20] J.I. Pankove, Optical Processes in Semiconductors, New York, Dover, 1971, p. 93.
[21] Y. Natsume, H. Sakata, Mater. Chem. Phys. 78 (2002) 170.
[22] R. Thielsch, A. Gatto, J. Heber, N. Kaiser, Thin Solid Films 410 (2002) 86.
[23] H. Hu, C. Zhu, Y.F. Lu, Y.H. Wu, T. Liew, M.F. Li, B.J. Cho, W.K. Choi, J. Appl. Phys. 94 (2003) 551.
[24] T. Tan, Z. Liu, H. Lu, W. Liu, H. Tian, Opt. Mater. 32 (2010) 432.
[25] M. Harris, H. Macleod, S. Ogura, E. Pelletier, B. Vidal, Thin Solid Films 57 (1979) 173.
[26] I.N. Sokolik, O.B. Toon, J. Geophys. Res. 104 (1999) 9423;
Refractive index data interpolation was prepared by B.W. Kimmel, Natural Phenomena Simulation Group, University of Waterloo, Canada, 2009.
[27] K. Sangwal, W. Kucharczyk, J. Phys. D: Appl. Phys. 20 (1987) 522.